Particulate Science and Technology, 21: 375–386, 2003

ISSN: 0272-6351
DOI: 10.1080/02726350390240223

Taylor & Francis
Taylor & Francis Group

Gas Flow and Particle Transport and Deposition in a Pilot-Scale Furnace

GOODARZ AHMADI
CHUNHONG HE

Department of Mechanical and Aeronautical Engineering
Clarkson University
Potsdam, New York, USA

DUANE H. SMITH
EVERETT RAMER

National Energy Technology Laboratory
U.S. Department of Energy
Morgantown, West Virginia, USA

The present work describes a computer simulation study of gas flow and particle transport and deposition in a pilot-scale furnace with cooling system. The Gambit code is used to generate the geometry and the computational grid. An unstructured mesh is generated for the pilot-scale boiler. The FLUENT code is used for evaluating the gas mean velocity, turbulence fluctuation energy, and mean pressure, as well as temperature fields and chemical species concentrations. The particle equation of motion includes the nonlinear drag, gravity, Brownian, lift, and thermophoretic forces. The gas velocity and thermal conditions in the furnace are studied. Ensembles of particle trajectories are generated and statistically analyzed. Particle deposition rates on different walls are evaluated, and the effect of particle size is studied.

Keywords: furnace flow, furnace temperature, particle transport, particle deposition, simulations

Introduction

Particle dispersion and deposition is of great concern in many industrial applications, including combustion, gas cleaning, microcontamination control, xerography, air pollution control, pneumatic transport, aerosol sampling, filtration, and separation processes. Coal boilers and furnaces are typical examples where particle dispersion and deposition play a critical role. Dispersion of particles greatly influences combustion processes including mixing and heat transfer, as well as pollutant formation, fouling, and slagging inside the boiler. The accumulation of deposits

The financial support of the U.S. Department of Energy (National Energy Technology Laboratory) is gratefully acknowledged. Thanks are also given to Dr. Simon P. Hanson of Consol Energy for many helpful discussions.

Address correspondence to Goodarz Ahamadi, Department of Mechanical and Aeronautical Engineering, Clarkson University, Potsdam, NY 13699-5725, USA. E-mail: ahmadi@clarkson.edu

derived from the mineral particles can cause blockage, erosion, and corrosion in the boiler and, as a result, lead to substantial financial losses.

Extensive reviews on aerosol transport and deposition in turbulent flows were provided by Friedlander (1977), Wood (1981), Hinds (1982), Hidy (1984), Papavergos and Hedley (1984), and Vincent (1995). In the turbulent gas flow condition, particles are convected by the mean motion and are dispersed by the fluctuating velocities. In the presence of a high temperature gradient field, particles experience a thermophoretic force as well as nonlinear drag, gravity, and Brownian forces.

Analyzing aerosol dispersion and deposition in a combustor has attracted considerable attention in recent years. Sanderson and Germane (1993) reported the experimental measurements of gas species concentration and particle composition in a combustor. Eatough (1991) designed a controlled profile reactor and collected a set of natural gas combustion data including gas species, temperature, and velocity measurements. Sommerfeld and Qiu (1993) studied particle dispersion in a pipe expansion nonreacting swirling flow using numerical simulations and phase-Doppler anemometry (PDA). Shirolkar and Queiroz (1993) developed a pulverized-coal combustion code to study particle dispersion in a axisymmetric reactor and compared their simulation results with the experimental data collected with a laser-based diagnostic technique. He and Ahmadi (1998) developed a Lagrangian particle tracking procedure to study particle dispersion and deposition in a combustor including the effects of thermophoresis. The mean flow field in the combustor was simulated using the stress transport model of the FLUENT code (*FLUENT5 User's Guide*, 1998).

Walsh et al. (1990) studied the effects of coal properties on particle deposition on a heat exchanger tube. Baxter (1993) predicted ash deposition during biomass and coal combustion. Ash deposition in an axisymmetric pilot-scale reactor was modeled by Richards et al. (1993). Boyd and Kent (1994) studied the role of burner swirl using the particle-tracking method and compared their results with experimental data. Yilmaz and Cliffe (1997) reported their simulation results for coal ash deposition onto a superheater tube. Most of these earlier works dealt with idealized axisymmetric geometries. Studies of particle transport and deposition in complex three-dimensional complex boilers and furnaces with chemical reactions and internal cooling systems are seldom reported.

In the present work, a computational modeling study of gas flow, heat transfer, and particle dispersion and deposition in the pilot-scale furnace with combustion is reported. The exact geometry of the furnace including its cooling system was meshed in the simulation. The $k - \varepsilon$ model of the FLUENT code was used for simulating the mean gas velocity, the turbulence fluctuation energy, the temperature field, and the chemical species concentrations in the furnace. A simple methane gas-oxygen reaction was used to model the combustion process. Soot particle trajectories were analyzed, and the deposition rates on different walls were evaluated.

Pilot-Scale Furnace

Figure 1 shows the geometry of the pilot-scale furnace used in this study. The furnace may be configured to simulate wall fired or tangentially fired conditions. For this study the case of tangentially fired low-NOX burners was analyzed. The air and coal inlets are positioned at five elevations, starting from the bottom, lower secondary air (LSA), primary air (PA)/coal, upper secondary air (USA), close-coupled

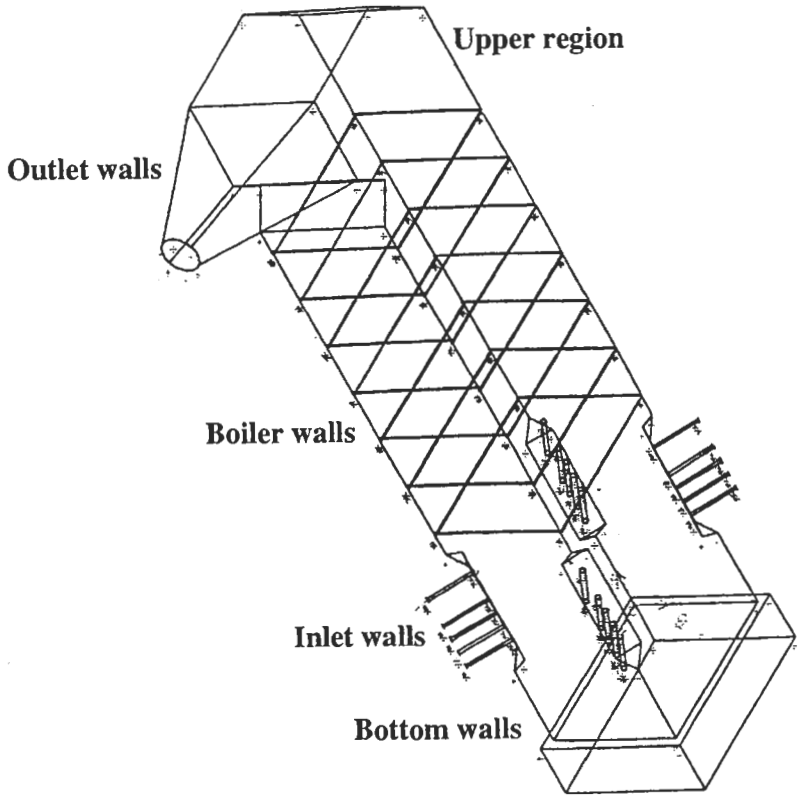

Figure 1. Geometry of a pilot-scale boiler.

overfire air (CCOFA), and separated overfire air (SOFA). Fuel is carried into the furnace by primary air at the second level. Air distribution was 30% LSA, 15% PA, 30% USA, 12.5% CCOFA, and 12.5% SOFA. At each level, air/coal was divided equally between four ports positioned at the corners. The diameter of the inlet tubes is one inch. Primary air temperature was 150°F (339 K). All other air feeds were at 600°F (589 K). At seven horizontal levels along the furnace, cooling tubes are placed that protrude into the flow. The diameter of the cooling tubes is 0.25 inch (0.635 cm); they are positioned at 0.25 inch (0.635 cm) away from the furnace wall. The walls of the furnace are also thermally insulated.

Computational Model

Geometry and Mesh Generation

The commercial mesh generator code Gambit of the FLUENT code was used to generate the three-dimensional geometry and an unstructured grid for the pilot-scale furnace. To achieve better grid resolution near the critical areas and boundaries, such as the 20 inlet ports at five levels and the 28 cooling tubes at seven levels, the geometries were created volume by volume. In total 15 volumes were created and connected by the joined face procedure. Each volume was then meshed separately. Grid adaptation was used, and, in particular, the grid near the inlet regions was modified and increased until no noticeable changes in the solution were obtained. The final unstructured grid that had 373,525 nodes and 529,920 elements was used in the simulation. Figure 2 shows the resulting computational surface grid of the furnace.

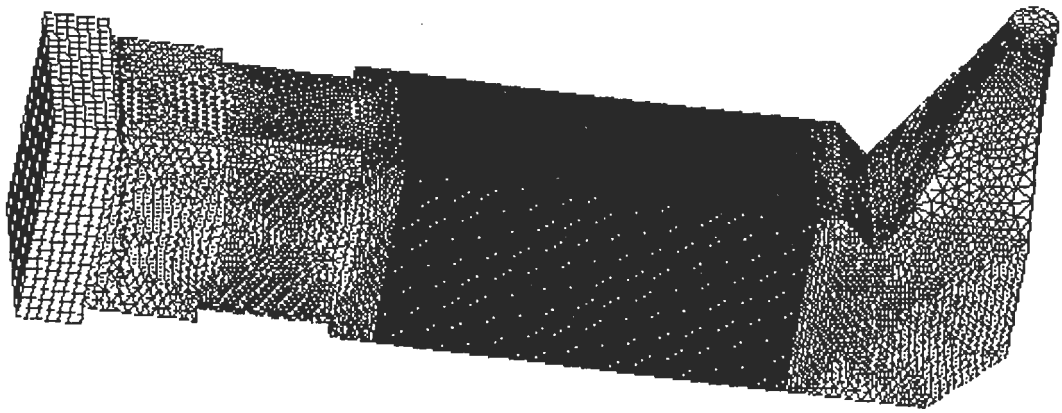

Figure 2. Computational surface grid of the pilot-scale boiler.

Gas Flow Simulation

Analysis of reacting flows is of interest for applications to liquid fuel and coal combustion in furnaces. The gas flow in the furnace is assumed to be compressible with heat transfer and includes radiation transport. The combustion process considered in this study is that of methane gas. The combustion is modeled as a single-step global chemical reaction of gaseous methane and oxygen to produce carbon dioxide and water vapor, i.e.,

$$CH_4 + 2O_2 \rightarrow CO_2 + 2H_2O$$

It should be emphasized that the pulverized coal combustion involves rather simple chemistry. In this study simple one-step chemistry was used to account for the heat generation, but the details of the combustion process were not accounted for.

The $k-\varepsilon$ turbulent model and P-1 radiation model of the FLUENT code (Version 5.0) were also used for the flow simulation. The FLUENT code provides options for using the $k-\varepsilon$ model, as well as other turbulence models. While the $k-\varepsilon$ model has certain limitations, it is widely used in industrial applications due to its simplicity and robustness. Details of the governing equations for the flow simulation may be found in the *FLUENT5 User's Guide* (1998).

Particle Trajectory Analysis

The equation of motion of a small particle, including the effects of nonlinear drag and gravitational forces, is given by

$$\frac{du_i^p}{dt} = \frac{3\nu C_D Re_p}{4d^2 S}\left(u_i - u_i^p\right) + g_i + f_i^T \tag{1}$$

and

$$\frac{dx_i}{dt} = u_i^p \tag{2}$$

Here, u_i^p is the velocity of the particle and x_i is its position, d is the particle diameter, S is the ratio of particle density to fluid density, g_i is the acceleration of gravity, v is the kinematic viscosity of the gas, and f_i^T is the thermophoretic force per unit mass.

The first term on the right-hand side of Equation (1) is the drag force due to the relative slip between the particle and the fluid. The drag force is, generally, the dominating force. The drag coefficient, C_D, is given as

$$C_D = \frac{24}{Re_p}, \quad \text{for } Re_p < 1 \tag{3}$$

and

$$C_D = \frac{24}{Re_p}\left(1 + \frac{1}{6}Re_p^{2/3}\right), \quad \text{for } 1 < Re_p < 400 \tag{4}$$

where Re_p is the particle Reynolds number defined as

$$Re_p = \frac{d|u_j - u_j^p|}{v} \tag{5}$$

The expression for the thermophoretic force, which depends on temperature gradient, is given in the FLUENT manual. Recent development on the thermophoretic force was discussed by He and Ahmadi (1998).

Equation (1) includes all the relevant forces and forms the basis for the discrete second-phase analysis of the FLUENT^{TM} code that was used in the present computation. This approach is based, in part, on the technique developed by Li and Ahmadi (1995). Effects of turbulence dispersion and thermophoresis on particle deposition rates on different surfaces were also studied.

The particle equation of motion used requires knowledge of the instantaneous turbulent fluid velocity at the location of each particle at every instant of time. As noted before, the mean liquid velocity was evaluated by the use of the $k - \varepsilon$ turbulence model and the fluctuation velocity components were calculated with the use of the discrete random model (DRW).

Particle Equation of Motion Results

Flow Simulation

In this section, gas flow simulation results for the pilot-scale furnace are described. The total airflow rate for the inlet ports (at five levels) was 1102 lb/hour (0.14 kg/s). An inlet turbulence intensity of 10% at the inlet was assumed. Table 1 lists the detailed boundary conditions for different inlet ports (at five levels) including airflow rate, velocity, temperature, and mass fraction of methane and oxygen. In addition, a temperature boundary condition of 100°F (311 K) for the cooling pipe was used. The thermal boundary conditions for the furnace are rather complicated. In these simulations, the furnace walls were assumed to be thermally insulated and have an emissivity of 0.7.

Table 1
Boundary conditions for inlet ports

	Airflow rate (kg/s)	Velocity (m/s)	Temperature (°F)	CH_4 Mass fraction	O_2 Mass fraction
Lower secondary air	0.042	41.68	589	0	0.22
Primary air/coal	0.021	20.84	339	0.4	0.22
Upper secondary air	0.042	41.68	589	0	0.22
Close-coupled overfire air	0.017	17.37	589	0	0.22
Separated overfire air	0.017	17.37	589	0	0.22

Figure 3 shows the velocity vector plots at different planes across the intake region in which the combustion occurs. It is observed that the flow field in the intake region of the furnace is rather complex. In particular, several strong recirculating regions due to tangentially fired inlet jets are clearly observed for the inlet angles assumed in this study.

Figure 4 shows the contours of velocity magnitude at the midsection of the furnace and two planes crossing the inlet pipe levels. The gas enters the furnace from inlet ports at different levels with high velocity. Strong mixing occurs in the intake region, and most of gas turns upward and enters the upper section of the furnace. The velocity is relatively high in the central part of the furnace near the intake region, of the order of 4 to 8 m/s. The velocity drops near the furnace sidewalls to about 1 to 2 m/s. The gas velocity near the outlet then increases to about 10 m/s due to the decrease in cross-sectional area.

Figure 5 shows the static pressure contours at the midsection of the pilot-scale furnace. It is observed that there is a pressure increase in the central part of the inlet region, but the pressure changes only slightly inside the furnace. The main pressure drop occurs at the furnace outlet region.

Variations of the turbulence kinetic energy at the plane crossing the midsection of the furnace are plotted in Figure 6. It is noticed that in the inlet region, the turbulence fluctuation energy is quite high, of the order of 20 to 30 m^2/s^2. Away

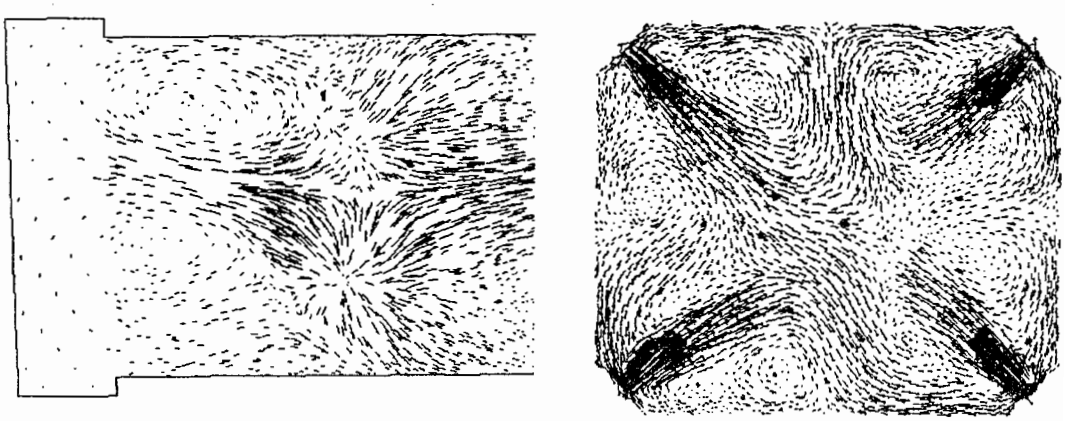

Figure 3. Velocity vector plots in the intake region of the boiler.

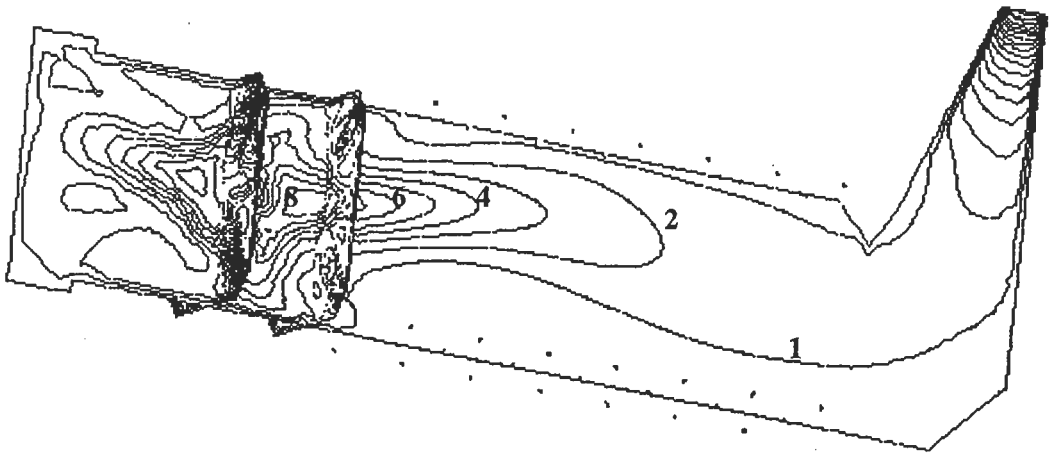

Figure 4. Velocity magnitude contour plots in the boiler. (The velocity magnitudes are in m/s.)

from the inlet region, the kinetic energy decreases rapidly. The kinetic energy drops to about 0.01 m^2/s^2 in the upper half of the furnace.

Figure 7 shows the temperature contours at the midsection of the furnace. It is observed that the gas temperature in the lower part of the furnace increases to about 2200 K due to the heat released from the combustion. The gas temperature near the upper walls reduces significantly to about 1500 K due to the effect of the cooling tubes. Near the cooling tubes there is a significant temperature drop, indicating a significant amount of heat transfer from the hot gas to the cooling tube. While detailed comparison with the experimental furnace was not possible, the temperature

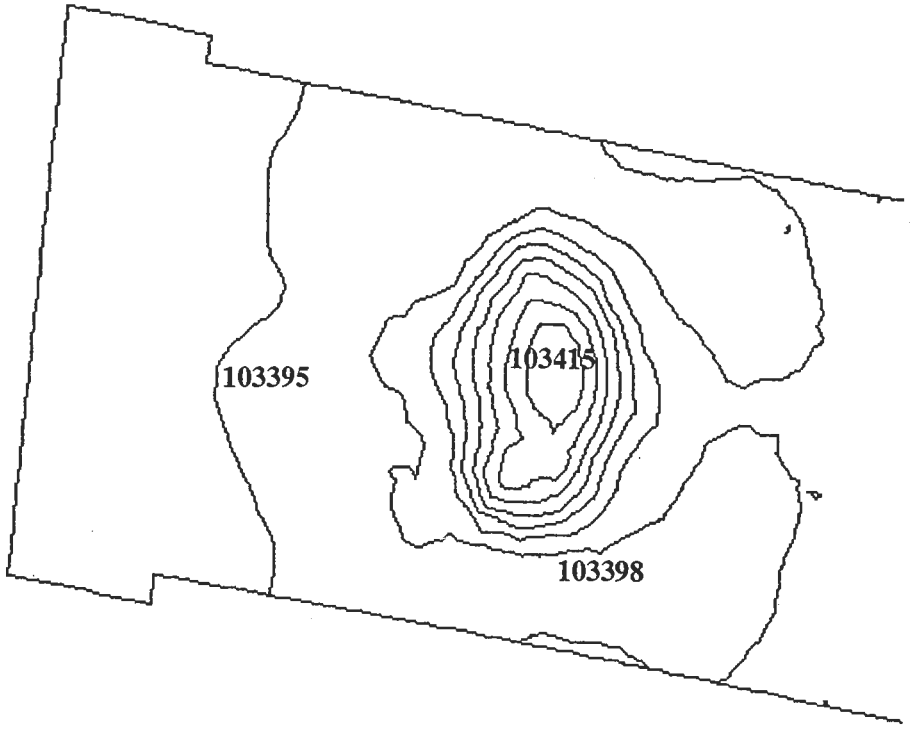

Figure 5. Pressure contour plots in the boiler intake region. (Pressure contours are in Pa.)

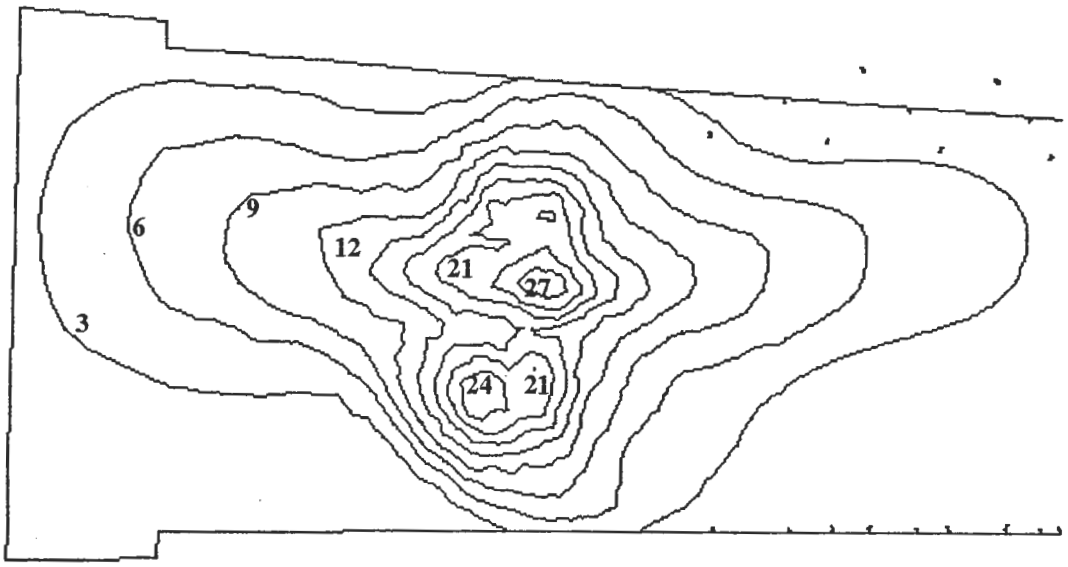

Figure 6. Turbulence kinetic energy contour plots in the boiler intake region. (Kinetic energy contours are in m^2/s^2.)

variation shown in Figure 7 was within the range of the experimental furnace. It should be emphasized that the radiation effects are quite important. When the radiation effect was neglected, the model predicted unrealistically high temperatures.

Figure 8 shows the contours for the mass fraction of CO_2 at the furnace midsection. The CO_2 is generated through the reaction of methane gas with oxygen. This figure shows that the mass fraction of CO_2 is roughly constant at about 0.16 in the main body of the furnace except at the inlet ports.

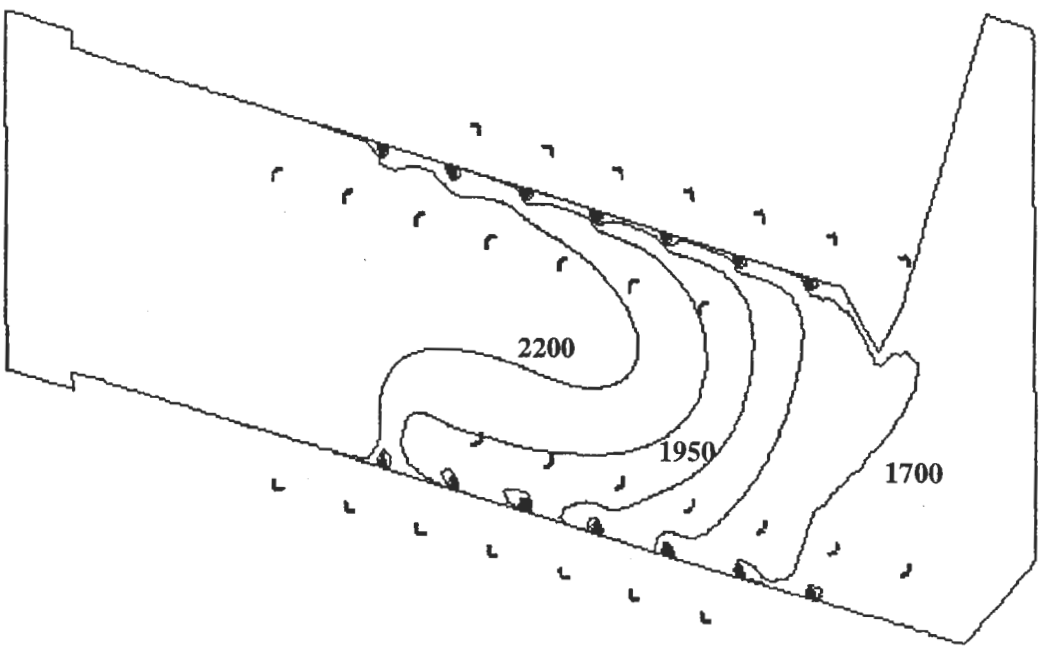

Figure 7. Temperature contour plots in the boiler midsection. (Absolute temperatures contours are in degree Kelvin.)

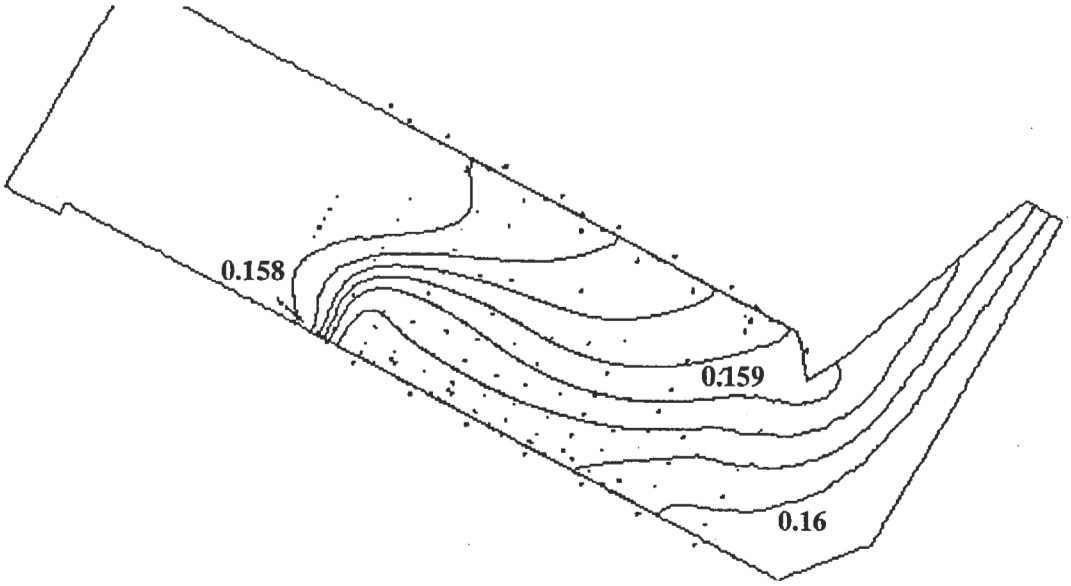

Figure 8. CO_2 mass fraction contour plots in the boiler midsection.

Particle Trajectories

In this section, particle transport and deposition in the pilot-scale furnace are discussed. Particles are assumed to originate from the primary air/fuel inlets. Particle initial velocities are assumed to be the same as the local mean fluid velocities. Sample trajectories for particles under the action of relevant forces and turbulence dispersion were studied.

Sample mean trajectories for 1 μm ash particles in the furnace in the absence of turbulence fluctuations are shown in Figure 9. Ash particles are assumed to have a density of 600 kg/m^3. It is observed that particles are carried into the furnace by the primary air/fuel jets following the mean flow streamlines. Some particles are captured by the recirculating eddies created by the oppositely fired inlet air jets, and a few particles deposit on the furnace walls in the inlet region. The rest of the particles enter the upper part of the furnace and continue to be transported upstream. Additional simulation results for 30 μm particles (not shown here due to space

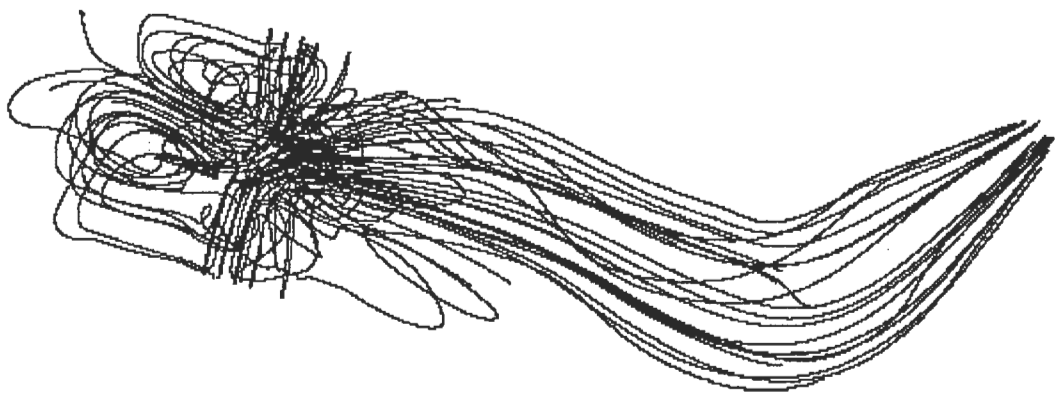

Figure 9. Sample particle trajectories in the absence of turbulence.

Figure 10. Sample particle trajectories in the presence of turbulence.

limitations) show that the general features of particle trajectories for different size particles are quite similar.

Figure 10 shows sample particle trajectories for 1 μm particles for the real situation when the effects of turbulence velocity fluctuations are included in the analysis. It is observed that the particles are dispersed significantly by the action of the gas turbulence. Most particles follow the mean streamlines, and many are captured by the recirculating eddies near the inlet. A number of particles escape from the furnace outlet, while many deposit on the furnace walls.

Comparison of Figures 9 and 10 indicates that particle trajectories under the mean flow condition (when turbulence is ignored) have significant differences from the case that turbulence dispersion is included. Clearly, turbulence plays an important role in particle dispersion and deposition processes. It is also observed that the number of deposited particles on the furnace walls increases significantly when turbulence fluctuation effects are included.

To study particle deposition patterns, 8000 particles were released from the primary air/fuel ports, and the numbers of deposited particles on the furnace walls were evaluated. It is assumed that when a particle touches the surface of a wall, it will deposit. Table 2 lists the number and percentages of deposited particles on different furnace surfaces for 1 and 30 μm particles. Various wall regions of the furnace are identified in Figure 1. For 1 μm particles, only about 16% of particles escape from the outlet. The amount of deposited particles on the cooling pipes, the outlet walls, the furnace upper region, the furnace midsection walls, the inlet walls, and the furnace bottom walls are, respectively, 1.6%, 3%, 4.1%, 18.9%, 26.2%, and 30.3%. Table 2 shows that a large number of particles tend to deposit on the furnace walls in the inlet and bottom wall regions. This is perhaps due to the strong recirculating eddies and high level of turbulence formed by the tangentially fired inlet jets. Comparing the distribution of deposited 1 and 30 μm particles, it is noticed that a

Table 2
Particle deposition rates on the furnace surfaces

	d = 1 μm		d = 30 μm	
Furnace surfaces	Depos. num.	Percentages	Depos. num.	Percentages
Outlet	1276	16.0%	1195	14.9%
Cooling pipes	125	1.6%	154	1.9%
Outlet walls	243	3.0%	215	2.7%
Upper region	326	4.1%	322	4.0%
Furnace walls	1515	18.9%	1405	17.6%
Inlet walls	2094	26.2%	2288	28.6%
Bottom walls	2420	30.3%	2421	30.3%

larger number of 30 μm particles deposited on the inlet walls. Also, a larger number of 1 μm particles escaped from the furnace outlet compared to that 30 μm particles. Table 2 also shows that the deposition patterns of 1 and 30 μm particles are quite similar. This indicates that turbulence dispersion dominates the particle deposition process in the furnace, and it overwhelms the particle inertial and gravity effects for the size range considered.

Conclusions

In this work, the simulation results for gas flow and particle dispersion and deposition in the modeled pilot-scale furnace were studied. The mean velocity, turbulence intensity, temperature field, and chemical species concentrations were simulated. Ensembles of trajectories for different size particles were generated and particle deposition rates on different regions were analyzed. On the basis of the presented results, the following conclusions are drawn:

- The gas flow field in the furnace can be quite complex and involves many recirculating flow regions.
- The turbulence fluctuation energy is quite high in the furnace inlet region, but drops significantly in the bulk of the furnace.
- The cooling pipes absorb a large amount of heat and significantly reduce the gas temperature in the upper part of the furnace.
- The simulation results show that the lower part of the furnace is dominated by the mixing, while strong temperature gradient occurs in the upper part of the furnace.
- Turbulence dispersion strongly affects particle transport and deposition processes in the furnace.
- General features of the deposition pattern for different size particles are quite similar.
- Particle deposition varies significantly in different parts of the furnace. Surfaces near the inlets and lower part of the furnace have the highest particle deposition, and upper furnace walls have the lowest.

It should be emphasized that the presented results were concerned with the mechanics of the flow and thermal conditions in the furnace. Additional complexity

of pulverized coal combustion chemistry and the features of cake buildup on the furnace wall are left for future studies.

References

Baxter, L. 1993. Ash deposition during biomass and coal combustion: A mechanistic approach. *Biomass Bioenergy* 4: 85–102.

Boyd, R. & J. Kent. 1994. Comparisons of large scale boiler data with combustion model predictions. *Energy Fuels* 8: 124–130.

Eatough, C. N. 1991. Controlled profile design and combustion measurements. Ph.D. diss., Mechanical Engineering Department, Brigham Young University, Provo, Utah.

FLUENT5 User's Guide. 1998. Version 5.01. Lebanon, N. H.: Fluent Inc.

Friedlander, S. K. 1977. *Smoke, Dust and Haze*, New York: John Wiley.

He, C., & G. Ahmadi. 1998. Particle deposition with thermophoresis in laminar and turbulent duct flows. *Aerosol Sci. Technol.* 29: 525–546.

Hidy, G. M. 1984. *Aerosols, An Industrial and Environmental Science*. New York: Academic Press.

Hinds, W. C. 1982. *Aerosol Technology: Properties, Behavior, and Measurement of Airborne Particles*. New York: John Wiley.

Li, A., & G. Ahmadi. 1995. Computer simulation of particle deposition in the upper tracheobronchial tree. *Aerosol Sci. Technol.* 23: 201–223.

Papavergos, P. G. & A. B. Hedley. 1984. Particle deposition behavior from turbulent flow. *Chem. Eng. Des.* 62: 275–295.

Richards, G., P. Slater, & J. Harb. 1993. Simulation of ash deposit growth in a pulverized coal-fired pilot scale reactor. *Energy Fuels* 7: 774–781.

Sanderson, D. K., & G. J. Germane. 1993. Composition of combustion gases and particles in a pulverized coal-fired reactor. *Energy Fuels* 7: 910–918.

Shirolkar, J. S., & M. Queiroz. 1993. Parametric evaluation of a particle dispersion submodel used in a two-dimensional, pulverized-coal combustion code. *Energy Fuels* 7: 919–927.

Sommerfeld, M. & H.-H. Qiu. 1993. Characterization of particle-laden, confined swirling flows by phase-doppler anemometry and numerical calculation. *Int. J. Multiphase Flow* 19: 1093–1127.

Vincent, J. H. 1995. *Aerosol Science for Industrial Hygienists*. Oxford: Pergamon.

Walsh, P., A. Sayre, D. Loehden, D. Monroe, J. Beer, & A. Sarofim. 1990. Deposition of bituminous coal ash on an isolated heat exchanger tube: Effects of coal properties on deposit growth. *Prog. Energy Combust. Sci.* 16: 327–345.

Wood, N. B. 1981. The mass transfer of particles and acid vapour to cooled surfaces. *J. Inst. Energy* 76: 76–93.

Yilmaz, S. & K. Cliffe. 1997. Simulation of coal ash deposition on/to a superheated tube. *J. Inst. Energy* 70: 17–23.